Effect of Metallic Wire Inserted in Nozzle in High-Speed Melt Spinning of Poly(ethylene terephthalate)

HYUNG JOONG JEON,[1] HIROSHI ITO,[1] TAKESHI KIKUTANI,[1] NORIMASA OKUI,[1] MIYOSHI OKAMOTO[2]

[1] Department of Organic and Polymeric Materials, Tokyo Institute of Technology, 2-12-1 O-okayama, Meguro-ku, Tokyo 152, Japan

[2] Toray Industries Inc., The Okamoto Research Laboratory, 2-2, Sonoyama 3-chome, Otsu-city, Shiga-Prefecture 520, Japan

Received 27 January 1998; accepted 7 March 1998

ABSTRACT: High-speed melt spinning of poly(ethylene terephthalate) was performed using a spinning nozzle with an inserted metallic wire of various lengths (0, 8, 30, and 45 mm). The molecular orientation of as-spun fibers increased with the increase in the wire length at all the take-up velocities examined. Along with the enhanced molecular orientation, the longer wire length led to the starting of orientation-induced crystallization at lower take-up velocities. The structure of crystallized fibers obtained at low speeds can be characterized by high crystallinity and relatively low molecular orientation. From the on-line measurement of the diameter and temperature profiles of the spin line with the 30-mm metallic wire, it was revealed that the spin-line had a maximum diameter of about 6 mm at the wire end. The spin-line temperature at this position was about 190°C. The solidification of the spin-line occurred at positions much closer to the spinneret in comparison with ordinary high-speed spinning. These results show that high-speed spinning with a wire inserted in the nozzle corresponds to a spinning process operated at extremely low extrusion temperature using a nozzle with an extremely large diameter. From the starting of orientation-induced crystallization at lower levels of birefringence in comparison with ordinary high-speed spinning, the alteration of the inherent fiber structure that cannot be represented by birefringence was also suggested. © 1998 John Wiley & Sons, Inc. J Appl Polym Sci 70: 665–674, 1998

Key words: high-speed spinning; orientation-induced crystallization; fiber structure; drawdown ratio

INTRODUCTION

High-sped melt spinning is a process in which significant fiber structure formation occurs. The structure formation can be represented basically by molecular orientation and orientation-induced crystallization; above a certain take-up velocity, highly oriented and crystallized fibers can be obtained. These fibers are applicable to end uses without any further drawing and annealing processes.

There have been many works on the high-speed spinning of poly(ethylene terephthalate) (PET) because PET is one of the most important fiber forming materials. These studies include the effects of take-up velocity,[1–6] mass-flow rate,[7,8] and some other spinning conditions[9–11] on the fiber structure formation, and the structure and properties of high-speed spun fibers prepared from modified PETs and copolyesters.[12–15] The effects of the mutual interaction of two components on the spinning dynamics and fiber structure formation in high-speed melt spinning of sheath-core type bicomponent fibers were also investigated through experimental and numerical

Journal of Applied Polymer Science, Vol. 70, 665–674 (1998)
 CCC 0021-8995/98/040665-10

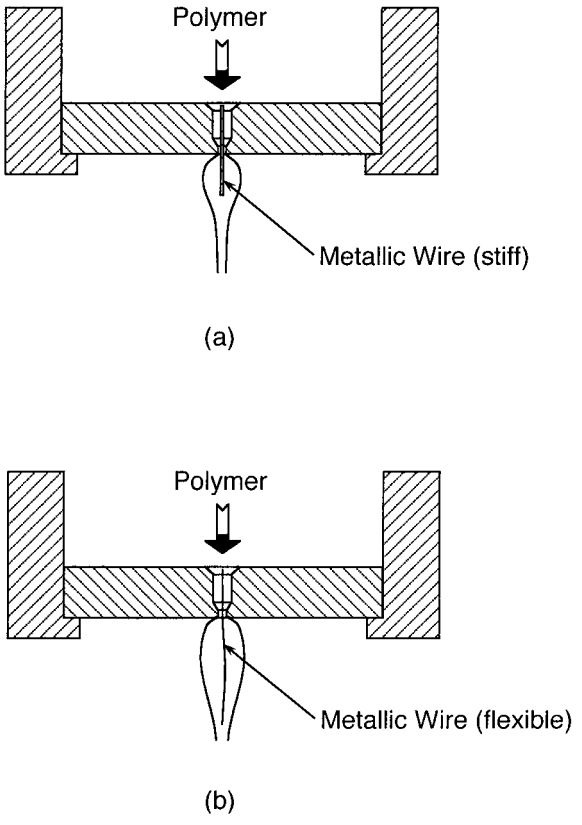

Figure 1 Schematic diagram of the nozzle with the inserted metallic wire. Two kinds of wire were used: (a) stiff and (b) flexible.

analyses.[16–18] There were many attempts to control the fiber structure formation through the alteration of the spinning process by a hot or cold tube[19,20] and a liquid isothermal bath.[21–23] Recently we investigated the effect of an extraordinary large nozzle diameter on the fiber structure formation.[24]

These analyses confirmed that if there is an enhancement of orientation-induced crystallization in the high-speed region through either the enhancement of the cooling effect or modification of polymers, it leads to higher crystallinity and relatively lower molecular orientation. The enhancement of crystallization is caused by the higher crystallization temperature. The suppression of molecular orientation is attributable to the reduction of the contribution of air-friction force on the spin-line stress at the solidification point. This is brought about by the upward shift of the position of crystallization in the spin line.

In order to significantly alter the spin-line dynamics in this study, a metallic wire was inserted in the spinning nozzle and the effect of wire length on the structure formation in high-speed melt spinning of PET was investigated. There are some patents on the effect of a pin inserted in the spinning nozzle.[25–27] Although these patents claimed to stabilize the spin line and the formation of high-modulus and thermally stable fibers, the details of the effect of the pin are not clear. Also, the length of the wire adopted in this study is much longer than that of the pin reported in these patents.

EXPERIMENTAL

Fiber Spinning

PET chips (supplied by Toray Industries, Inc.; T-200T, $[\eta] = 0.632$ dL/g) were used for the high-speed melt spinning. The polymer was dried at 140°C for 3 days before the spinning experiment. Four kinds of spinnerets were prepared. Each spinneret had a single nozzle with an inserted metallic wire. Two of these had a thick and stiff stainless wire carefully placed at the center of the nozzle. The lengths of the wire protruding from the surface of the spinneret were 0 and 8 mm. The other two had a thin and flexible stainless wire that could move freely in the nozzle. The lengths of the wire were 30 and 45 mm. Schematic diagrams of these spinnerets are shown in Figure 1. The details of the spinneret sizes are also summarized in Table I.

In the cases of the spinnerets with relatively long wire length, it was difficult to initiate the extrusion under the usual procedure. Therefore, a hot tube was set beneath the spinneret before starting the extruder and a metering pump (Musashino Kikai, Co. Ltd.). After the stabilization of the spin line, the hot tube was removed. Then spinning was performed using a high-speed winder at least 5 min after the removal of the hot tube, which was assumed to be a sufficient time

Table I Specification of Spinnerets

Nozzle		Wire		
D	*L*/*D*	Material	Diameter (mm)	Length[a] (mm)
0.5 mm	2	Stainless steel	0.2	0
				8
		Brass	0.1	30
				45

[a] Protruding from the spinneret surface.

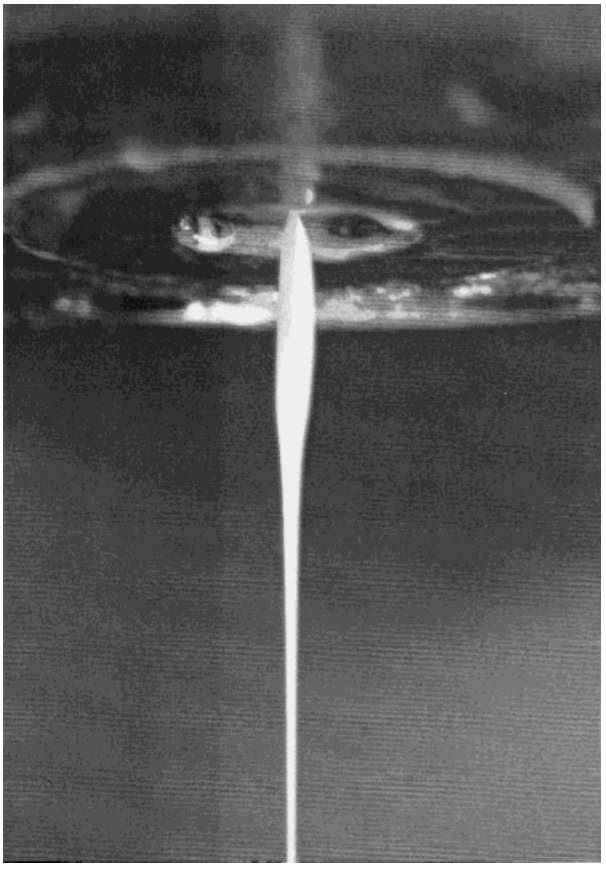

Figure 2 The photograph of the spin line near the spinneret for the wire length of 30 mm.

period for the spin line to become a new steady state without the hot tube.

The photograph of the spin line near the spinneret for the wire length of 30 mm is shown in Figure 2. The diameter of the spin line enlarged abruptly at the outlet of the nozzle, kept its size to the end point of the metallic wire, and then attenuated steeply. Both the stiff and flexible wires appeared to remain at the center of the molten filaments along the entire length of the wire.

The spinning conditions are summarized in Table II. Under these conditions, it was not possible to extrude the filament with a wire longer than 45 mm.

Measurements

Birefringence

The refractive indices parallel and perpendicular to the fiber axis were measured using an interference microscope (Carl Zeiss, Jena) equipped with a polarizing filter. The birefringence was calculated as the difference between two refractive indices. The results are an average of the measurement of 10 individual fibers.

Density

The density of the samples was measured at 25°C using a density gradient column prepared from *n*-heptane and carbon tetrachloride. Measurement was done 24 h after the immersion of samples into the column.

Differential Scanning Calorimetry (DSC)

The DSC measurement was performed using DSC-50 (Shimadzu) at the heating rate of 10 K/min. Prior to the measurement, the as-spun fibers were cut to powderlike short fibers. The weight of the samples were about 2.0–2.5 mg. The cold crystallization peak temperature and the melting peak temperature were analyzed from the DSC thermograms.

Wide Angle X-ray Diffraction (WAXD)

The WAXD studies of as-spun fibers were carried out using a Rigaku Denki X-ray diffractometer equipped with a position sensitive proportional counter. A nickel-filtered CuKα radiation source was used, and the equatorial intensity distribution was obtained from 5° to 35°.

Tensile Test

The load versus elongation curves of the fiber samples were obtained using a tensile test ma-

Table 2 Spinning Conditions for High-Speed Melt Spinning of PET

Polymer	PET (Toray, $[\eta]$ = 0.632 dL/g)
Mass-flow rate (g/min hole)	2.0
Spinning temperature (°C)	290
Take-up velocity (km/min)	
0- or 8-mm wire	1–5
30-mm wire	0.5–3.5
45-mm wire	0.5–2.0

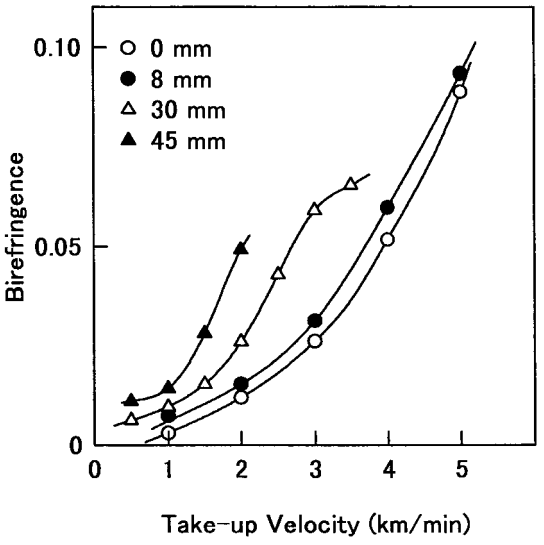

Figure 3 Relation between birefringence and take-up velocity for various wire lengths.

chine (UTM Zwick, 1425) at room temperature. The gauge length was 50 mm, and the tensile speed was 40 mm/min. The initial modulus, tenacity, and elongation at break were analyzed from the obtained load–elongation curves.

On-Line Measurement of Spin-Line Diameter and Temperature

On-line measurement of the spin-line diameter was performed using a diameter monitor (Zimmer, 460 A/2) at various take-up velocities and for the 0- and 30-mm wire lengths.

On-line measurement of the spin-line temperature near the spinneret was also performed using an IR radiation gauge[28] (Japan Sensor Corporation, TSS-15STTU) at the take-up velocity of 1 km/min and for the wire length of 30 mm.

RESULTS AND DISCUSSION

Structure and Properties of As-Spun Fibers

Birefringence and Density

Figure 3 shows the birefringence of fibers spun under various spinning conditions. The birefringence increased with an increase in the take-up velocity, and the longer wire length yielded the steeper increase in the birefringence. In cases of the wire length of 0 and 8 mm, the birefringence kept increasing up to 5 km/min. On the other hand, in cases of the wire length of 30 and 45 mm, it showed a tendency of saturation near the attainable maximum take-up velocities.

Figure 4 shows the changes of density of as-spun fibers with take-up velocity. The density was low and virtually constant at lower take-up velocities, indicating that the fibers are essentially amorphous, and then started to increase at a certain take-up velocity. An increase in the density indicates the occurrence of the orientation-induced crystallization in the spin line. The starting point of the density increment shifted to lower take-up velocities with an increase in the wire length. This means that the orientation-induced crystallization was significantly promoted by the use of long wire. The crystallization started even at around 1.5 km/min when the 45-mm wire was used.

WAXD

The WAXD diagrams of the fibers spun under various spinning conditions are shown in Figures 5, 6, 7, and 8. Comparing each WAXD diagram, it was confirmed that distinct crystalline reflections started to appear at lower take-up velocities with an increase in the wire length. The result for 45-mm wire showed especially distinct crystalline reflections at the take-up velocity of 2 km/min at which the conventional fibers are essentially amorphous. The velocity of the starting of orientation-induced crystallization observed in the WAXD diagrams is in good accordance with the results of the density measurements.

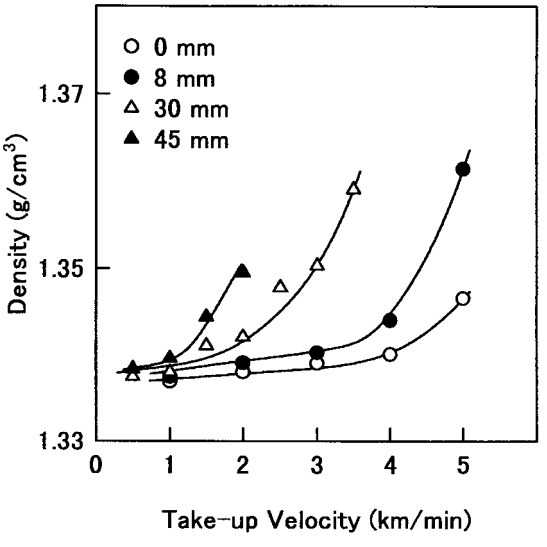

Figure 4 Relation between density and take-up velocity for various wire lengths.

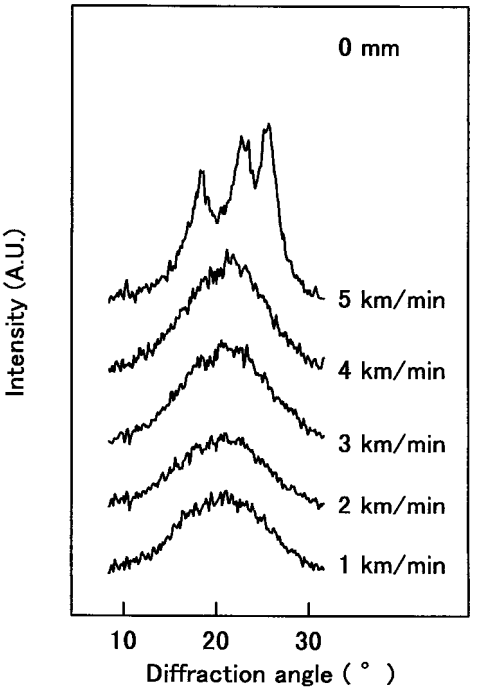

Figure 5 Equatorial WAXD intensity diagrams for fibers spun with a wire length of 0 mm.

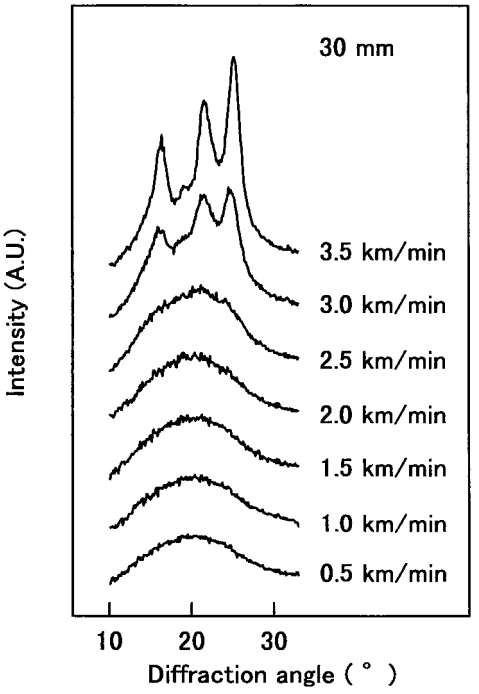

Figure 7 Equatorial WAXD intensity diagrams for fibers spun with a wire length of 30 mm.

DSC

The results of DSC measurements for the fibers spun under various spinning conditions are shown in Figures 9 and 10. Figure 9 shows the change in cold crystallization peak temperature (T_{cc}) with increasing take-up velocity. The T_{cc}

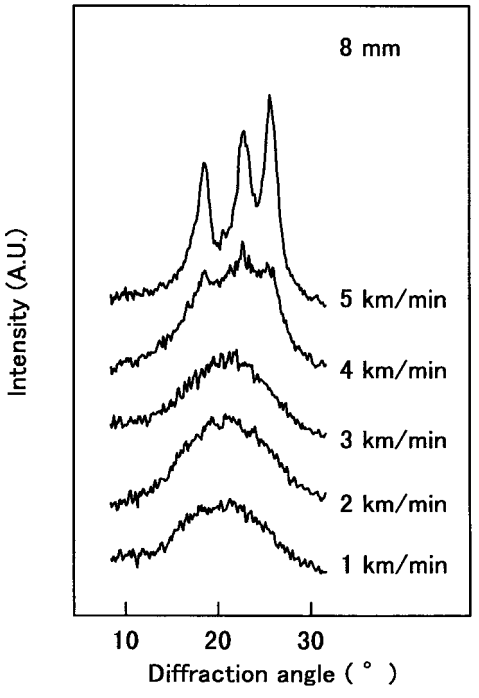

Figure 6 Equatorial WAXD intensity diagrams for fibers spun with a wire length of 8 mm.

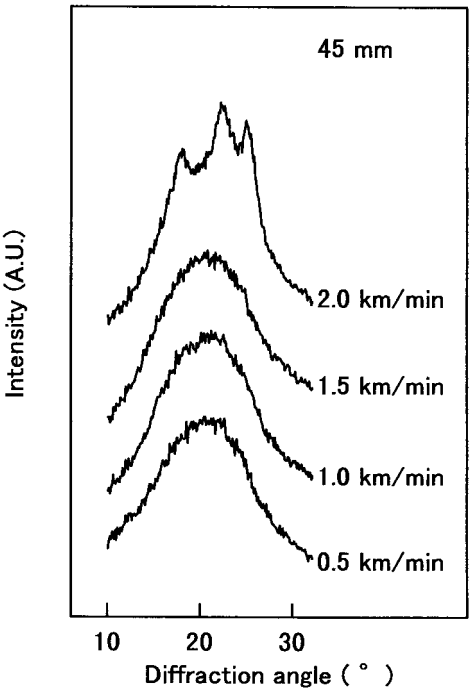

Figure 8 Equatorial WAXD intensity diagrams for fibers spun with a wire length of 45 mm.

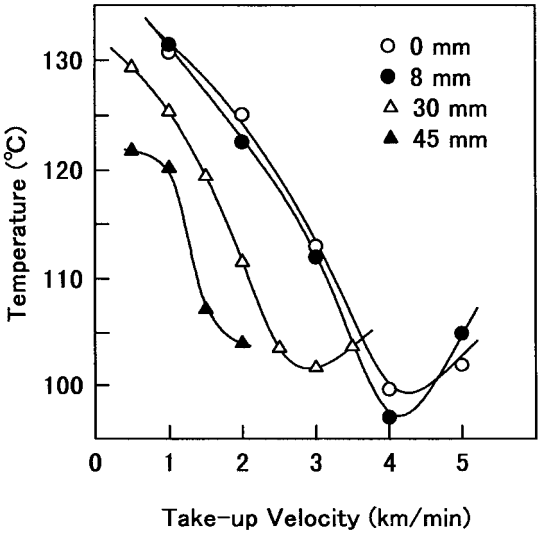

Figure 9 Relation between cold crystallization temperature and take-up velocity for various wire lengths.

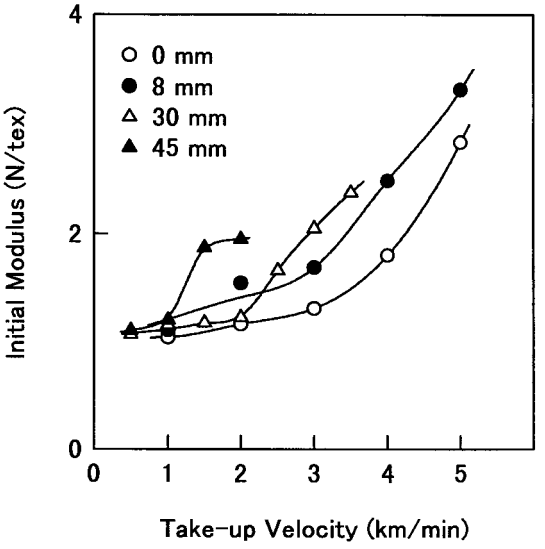

Figure 11 Change of initial Young's modulus analyzed from the load–elongation curves with take-up velocity and wire length.

observed in the heating process of the DSC measurements generally decreases with an increase in the take-up velocity.[1] The lower T_{cc} is due to the increase in crystallization rate caused by molecular orientation. The T_{cc} showed a lower value with an increase in the wire length. This result indicates the enhancement of molecular orientation and agrees with the results of the birefringence.

After the onset of orientation-induced crystallization, a small cold crystallization peak was still observed for all the wire lengths and its temperature increased slightly. These results indicate that the crystallized fibers have relatively low amorphous orientation. Selective incorporation of highly oriented molecules into the crystals in the course of orientation-induced crystallization might be the reason for the decrease of amorphous orientation and consequently the increase of cold crystallization temperature.

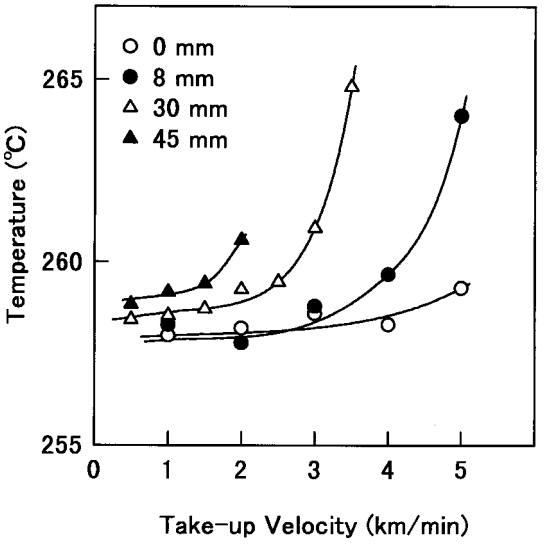

Figure 10 Relation between melting temperature and take-up velocity for various wire lengths.

Changes in melting temperature (T_m) with increasing take-up velocity are shown in Figure 10. It was reported that the T_m of high-speed spun PET fibers starts to increase at a take-up velocity where the orientation-induced crystallization begins.[29] From this viewpoint, the starting point of the T_m increment agrees well with the results of the density and WAXD measurements.

It is also interesting to note that the melting points of the fibers before the onset of orientation-induced crystallization in the spin line are slightly different, depending on the wire length. This result suggests that the crystal structures formed in the DSC heating process are different. In other words, an inherent structural difference aside from the birefringence may exist in the amorphous fibers prepared with different wire lengths.

Tensile Test

The initial Young's modulus and elongation to break analyzed from the load–elongation curves of the fibers spun under various spinning conditions are shown in Figures 11 and 12. An increase

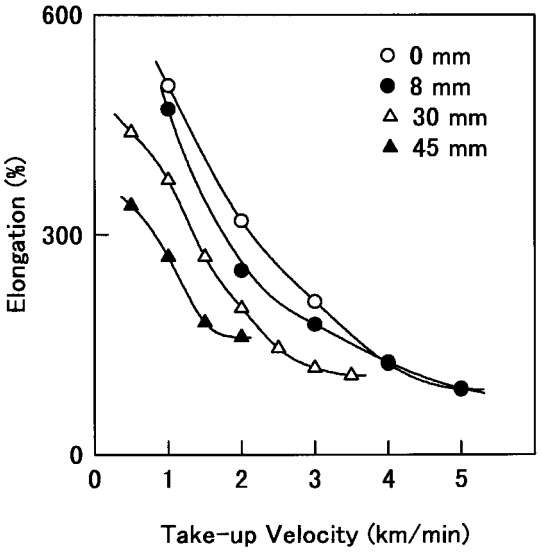

Figure 12 Change of elongation at break analyzed from the load–elongation curves with take-up velocity and wire length.

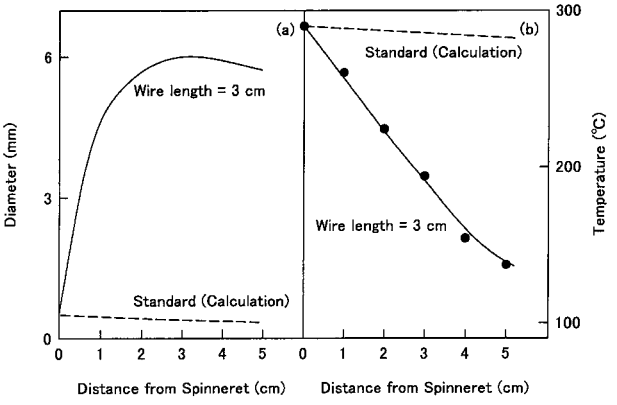

Figure 14 (a) Diameter profile and (b) temperature profile for spin line with a wire inserted in the nozzle. (take-up velocity = 1 km/min). Diameter and temperature profiles for ordinary spinning obtained from numerical simulation are plotted for comparison.

in the Young's modulus and a decrease in the elongation to break accompanied by the increase in the take-up velocity were more prominent for the fibers prepared with longer wire lengths. These results are in good accordance with the structural difference observed in as-spun fibers.

Figure 13 shows the tenacity of the fibers obtained under various spinning conditions. Although the tenacity increased with the take-up velocity, the difference between the fibers prepared with different wire lengths is significantly smaller than in the cases of Young's modulus, elongation to break, and other structural parameters. Because of the tendency toward saturation at higher take-up velocities, the fibers prepared with longer wire lengths tended to show lower tenacity. This result may be another indication of the inherent difference in the fibers spun with different wire lengths as was discussed for the melting point of amorphous fibers in the DSC analysis. A similar structural difference was suggested by Brody[30] in the comparison of high-speed spun fibers and conventional fibers.

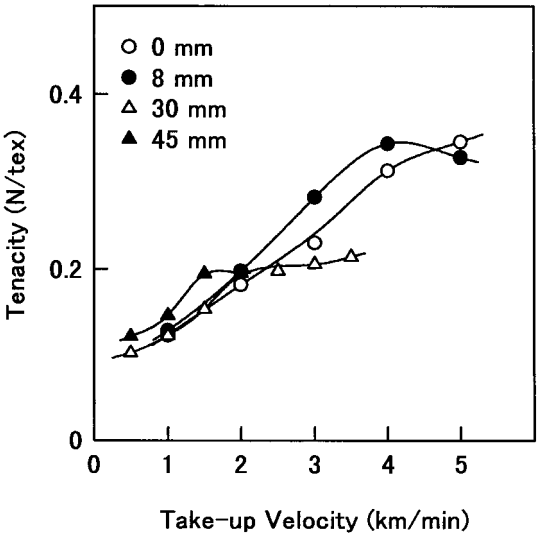

Figure 13 Change of tenacity analyzed from load–elongation curves with take-up velocity and wire length.

Spinning Behavior

In order to understand the mechanism of fiber structure development in the melt spinning process with a metallic wire inserted in the spinning nozzle, on-line measurements of the fiber diameter and temperature profiles were performed in the spin line. The diameter profile near the spinning nozzle for the 1 km/min spin line with a 30-mm wire was analyzed from the photograph shown in Figure 2 and plotted in Figure 14(a). The diameter profile for the ordinary spinning obtained from the numerical simulation of the spinning process is also shown in the figure for comparison.[31] The spin-line diameter enlarged to about 6 mm at the end point of the wire. This was obviously induced by the disturbance of polymer flow caused by the shear stress acting at the interface between the wire and polymer. From the volume of the polymer on the wire it was estimated that it takes about 25 s for the polymer to

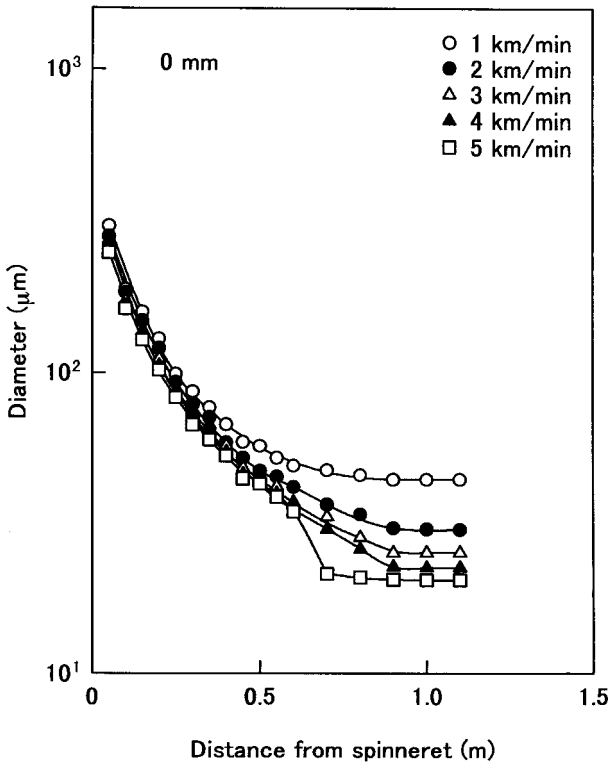

Figure 15 Diameter profiles of the spin line for the wire length of 0 mm.

flow from the outlet of the spinneret to the wire end, which is 30 mm below the spinneret. This is more than 100 times longer than in ordinary spinning. If cooling behavior is considered as a function of the distance from the spinneret, the longer residence time may lead to the significant enhancement of the cooling of the spin line.

To verify the cooling effect caused by the wire, on-line measurement of the spin-line temperature was performed at the take-up velocity of 1 km/min and with the wire length of 30 mm. The temperature profile from 1 to 5 cm below the spinneret is shown in Figure 14(b). From this measurement it was confirmed that the spin-line temperature cooled from 290°C to about 190°C at the wire end and to about 130°C at 5 cm below the spinneret. The calculated cooling behavior in the ordinary spinning process is also shown in Figure 14(b) for comparison. These results indicate that the major part of the attenuation of the spin line with metallic wire occurs at much lower temperatures in comparison with the ordinary melt spinning process.

The overall diameter profiles of the spin line for the wire lengths of 0 and 30 mm are shown in Figures 15 and 16. With the wire length of 0 mm and up to the take-up velocity of 4 km/min, the solidification of the spin line occurred at about 90 cm below the spinneret. At 5 km/min the solidification position shifted upward to about 70 cm. Immediately above the solidification position, the necklike deformation was observed, indicating the starting of orientation-induced crystallization.

By changing the wire length from 0 to 30 mm, the attenuation of the spin line became much steeper and the solidification position shifted upward. Up to the take-up velocity of 2.5 km/min, the solidification position was at about 50 cm below the spinneret. From 3 km/min, at which onset of the orientation-induced crystallization was confirmed from the structural analyses of the as-spun fibers, the necklike deformation started to occur and the solidification position moved upward. At 3.5 km/min the solidification position was only 20 cm below the spinneret. These changes in diameter profiles were obviously caused by the significant cooling of the spin line near the spinneret. Considering these results, the melt spinning with a metallic wire inserted in the nozzle can be regarded as a spinning process operated at extremely low spinning temperature using a spinning nozzle with an extremely large diameter.

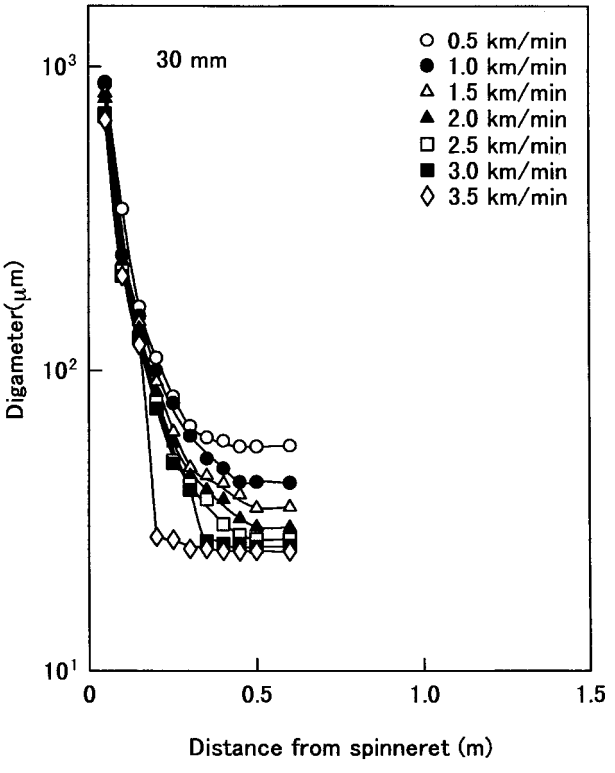

Figure 16 Diameter profiles of the spin line for the wire length of 30 mm.

Mechanism of Structure Formation Enhancement

The structural analyses of the as-spun fibers confirmed that the molecular orientation of the fibers was enhanced by using the nozzle with the inserted wire. Because of this enhanced molecular orientation, orientation-induced crystallization started to occur at lower take-up velocities. The promotion of the fiber structure development became more significant by extending the wire length.

As discussed previously, the melt spinning using a nozzle with an inserted wire corresponds to a condition with low spinning temperature and a large nozzle diameter. The theoretical consideration of the spin-line dynamics established by Kase and Matsuo[32] confirmed that spin-line stress increases with decreasing spinning temperature.[31] If the stress-optical law can be applied, higher spin-line stress directly relates to the higher molecular orientation of as-spun fibers and leads to the enhancement of orientation-induced crystallization. In our previous study of the spinning process using a spinning nozzle with an extraordinary large diameter, it was also confirmed that the orientation-induced crystallization is promoted along with the enhanced molecular orientation.[24] Therefore, the combination of these two effects (i.e., low spinning temperature and large nozzle diameter) might be the reason for the significant enhancement of the molecular orientation and orientation-induced crystallization. In these considerations, we neglected the effect of shear flow at the wire surface on the structure development because, even though there is a significant decrease in the polymer temperature, the flow itself is extremely slow and naturally the shear stress should also be low.

The relation between birefringence and density of the as-spun fibers is shown in Figure 17. The density increment started to occur at lower birefringences with an increase in the wire length. In other words, the structure of fibers prepared using the metallic wire can be characterized by high crystallinity and relatively low molecular orientation. This result indicates that the orientation-induced crystallization is not simply governed by molecular orientation represented by birefringence. This also suggests the difference in the inherent fiber structure prepared with different wire lengths as was discussed for the results of the melting temperature and tenacity measurements.

If the maximum spin-line diameter at the wire end is regarded as the initial diameter, the drawdown ratio of the spin line reaches about 20,000 in the spinning with a 30-mm wire and at the take-up velocity of 1 km/min. This value is about 100 times larger than that in the ordinary spinning process. Another important point is that this extreme drawdown occurs in a relatively low temperature region. These factors might have a significant affect on the alteration of the inherent fiber structure (e.g., network structure) and yield the enhancement of orientation-induced crystallization at lower levels of birefringence.

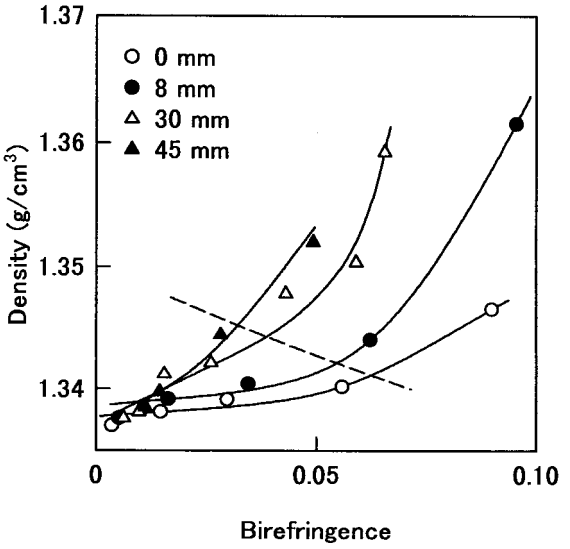

Figure 17 Relation between density and birefringence for various wire lengths. (- - -) The onset point of orientation-induced crystallization.

CONCLUSION

In the melt spinning of PET using a nozzle with an inserted metallic wire, the molecular orientation and orientation-induced crystallization of as-spun fibers were promoted. The structure of crystallized fibers obtained at low speeds can be characterized by high crystallinity and relatively low molecular orientation. The on-line measurement of the diameter and temperature profiles of the spin line with the 30-mm metallic wire revealed that the spin line had a diameter of about 6 mm and a temperature of about 190°C at the wire end. At the take-up velocity of 3.5 km/min, the solidification of the spin line caused by orientation-induced crystallization occurred at a position only 20 cm below the spinneret. High-speed spinning with a wire inserted in the nozzle corresponds to a spinning process operated at extremely low extrusion temperature using a nozzle with an extremely large diameter. These two factors had a

significant affect on the promotion of fiber structure development. On the other hand, the starting of orientation-induced crystallization at lower levels of birefringence suggested an alteration of the inherent fiber structure that cannot be represented by the birefringence.

REFERENCES

1. A. Ziabicki and H. Kawai, Eds., *High-Speed Fiber Spinning,* Wiley, New York, 1985.
2. J. Shimizu, K. Toriumi, and K. Tamai, *Sen'i Gakkaishi,* **33,** 5 (1977).
3. H. H. George, A. Holt, and A. Buckley, *Polym. Eng. Sci.,* **23,** 96 (1983).
4. K. Fujimoto, K. Iohara, S. Ohwaki, and Y. Murase, *J. Polym. Sci.,* **42,** 1509 (1991).
5. M. Iwata, K. Kamide, T. Kuriki, and T. Matsuo, *Sen'i Kikai Gakkaishi,* T245 (1992).
6. J. Shimizu, T. Kikutani, A. Takaku, and N. Okui, *Sen'i Gakkaishi,* **40,** T-63 (1984).
7. J. Shimizu, N. Okui, A. Kaneko, and K. Torium, *Sen'i Gakkaishi,* **34,** T-64 (1978).
8. K. Nakayama, S. Yamamoto, R. Ono–Oka, E. Aoki, T. Kurita, Y. Suda, and H. Kanetsuna, *Sen'i Rengokenkyukai,* **11,** 12 (1988).
9. C. T. Kiang and J. A. Cuculo, *J. Appl. Polym. Sci.,* **46,** 55 (1992).
10. G. Y. Chen, J. A. Cuculo, and P. A. Tucker, *J. Appl. Polym. Sci.,* **44,** 447 (1992).
11. R. K. Gupta and K. F. Auyeung, *J. Appl. Polym. Sci.,* **34,** 2469 (1987).
12. T. Kikutani, K. Morohoshi, H. Y. Yoo, S. Umemoto, and N. Okui, *Polym. Eng. Sci.,* **35,** 942 (1995).
13. S. Aslan, P. Laurienzo, M. Malinconico, E. Martuscelli, F. Pota, R. Bianchi, G. D. Dino, and G. Giannotta, *J. Appl. Polym. Sci.,* **55,** 57 (1995).
14. H. Yamada, T. Kikutani, A. Takaku, and J. Shikizu, *Sen'i Gakkaishi,* **44,** 177 (1988).
15. T. Kikutani, H. Yamada, A. Takaku, and J. Shimizu, *Sen'i Gakkaishi,* **44,** 317 (1988).
16. T. Kikutani, S. Arikawa, A. Takaku, and N. Okui, *Sen'i Gakkaishi,* **51,** 408 (1995).
17. T. Kikutani, J. Radhakrishnan, S. Arikawa, A. Takaku, N. Okui, X. Jin, F. Niwa, and Y. Kudo, *J. Appl. Polym. Sci.,* **62,** 1913 (1996).
18. J. Radhakrishnan, T. Kikutani, and N. Okui, *Text. Res. J.,* **67,** 684 (1997).
19. T. Kikutani, J. Radhakrishnan, M. Sato, N. Okui, and A. Takaku, *Int. Polym. Process.,* **XI,** 42 (1996).
20. T. Kikutani, K. Miyata, and N. Okui, in *Proceedings of the International Symposium on Fiber Science and Technology,* ISF '94, 1994, p. 18.
21. Q. Zhou, G. Wu, P. A. Tucker, and J. A. Cuculo, *J. Polym. Sci.,* **33,** 909 (1995).
22. K. Hayashi, K. Tani, H. Ishihara, and H. Yasuda, *Sen'i Gakkaishi,* **48,** 541 (1992).
23. H. J. Jeon, H. Ito, T. Kikutani, and N. Okui, *Sen'i Gakkai Prepr.,* 1997(G) 215, (1997).
24. H. J. Jeon, H. Ito, T. Kikutani, and N. Okui, *Sen'i Gakkaishi,* **53,** 540 (1997).
25. Jpn. Pat. *shou* 62-170513 (1987).
26. Jpn. Pat. *hei* 1-271817 (1989).
27. Jpn. Pat. *hei* 3-77286 (1991).
28. T. Kikutani, Y. Kawahara, T. Matsui, A. Takaku, and J. Shimizu, *Seikei-Kakou,* **1,** 333 (1989).
29. J. Shimizu, N. Okui, and T. Kikutani, *Sen'i Gakkaishi,* **34,** T-93 (1978).
30. H. Brody, *J. Macromol. Sci.-Phys.,* **B22,** 19 (1983).
31. T. Kikutani, *Kobunshi Fukugozairyou no Seikeikakou,* K. Funatsu, Ed., Shinzansha Saitekku, Tokyo, 1992.
32. S. Kase and T. Matsuo, *J. Appl. Polym. Sci.,* **11,** 251 (1967).